

SHAPE AND REFLECTANCE RECONSTRUCTION IN UNCONTROLLED ENVIRONMENTS BY DIFFERENTIABLE RENDERING

Rui Li, Guangming Zang, Miao Qi, Wolfgang Heidrich

King Abdullah University of Science and Technology
{rui.li, guangming.zang, miao.qi, wolfgang.heidrich}@kaust.edu.sa

ABSTRACT

Simultaneous reconstruction of geometry and reflectance in uncontrolled environments remains a challenging problem. In this paper, we propose an efficient method to reconstruct the scene’s 3D geometry and reflectance from multi-view photography using conventional hand-held cameras. Our method automatically builds a virtual scene in a differentiable rendering system that roughly matches the real world’s scene parameters, optimized by minimizing photometric objectives alternatingly and stochastically. With the optimal scene parameters evaluated, photo-realistic novel views for various viewing angles and distances can then be generated by our approach. We present the results of captured scenes with complex geometry and various reflection types. Our method also shows superior performance compared to state-of-the-art alternatives in novel view synthesis visually and quantitatively.

Index Terms— differentiable rendering, 3D reconstruction, viewpoint synthesis

1. INTRODUCTION

An object’s appearance is affected by many internal and external factors, including 3D geometry, surface reflection, and transmission, environmental lighting conditions, viewing angle, or camera position, etc. We call all of these the scene parameters. To estimate the scene parameters from multi-view photograph is a emerging and challenging task. It involves several inter-connected sub-problems, many previous works are focusing on recovering one of those parameters. To name a few: 3D shape reconstruction [1, 2, 3], image-based rendering [4, 5, 6], spatially-varying bidirectional reflectance distribution functions (SVBRDF) acquisition [7, 8], environment lighting estimation [9, 10], structure from motion [11], multi-view stereo [12], shading and stereo [13], reconstructing textured meshes [14], etc.

Different from explicit representation of 3D scene or viewpoint, representing 3D scene by implicit function or neural network (e.g., SRN [15], NeRF [16], pixelNeRF[17], NSVF [18], MipNeRF [19]) has gained popularity recently by a implicit volume (neural network), and optimizes scene volume via training a self-supervised neural network.

Differential rendering becomes another promising categories for 3D geometry optimization, texture mapping, novel view rendering. Liu et al. [1] propose a differentiable rendering framework that directly forward render colored mesh and back-propagate gradient to mesh vertices, color, silhouette, etc. Nimier-David et al. [20] proposed a physically-based engine, Mitsuba2, for estimating parameter gradient that based on Monte-Carlo sampling, thus, enables back propagating geometry, and other general scene parameters gradient flow.

However, directly optimizing scene parameters especially geometry structure of wild scene is still a challenging problem, experiments show the limited toy cases for directly optimization of geometry. Specifically, there are several technical challenges: first, accurate 3D geometry is unknown or requires an expensive 3D scanner. Second, specular reflection is shape-sensitive having a significant influence on object appearance. Finally, the natural environment contains multiple direct light sources and an indirect ray path, which is unknown and hard to direct.

To overcome the above technical challenges and enable reconstruction in a typical user scenario, we propose a systematic scene parameter reconstruction method that jointly estimates 3D geometry, surface reflectance, specular coefficients, camera pose, position, and lighting condition using a differentiable inverse rendering framework. Note that there are no specific requirements for the the photography acquisition process, i.e., it only requires several multi-view photos or surround video, without extra constraints such as controlled lighting, camera position or exposure, or a specific environment setup, to enable in-the-wild reconstruction.

Our contributions are listed as follows, (1) we propose a general parameterized framework to describe typical object appearance, enabling the direct reconstruction of a realistic scene from real-world multi-view photography for uncontrolled lighting conditions and general diffuse and specular scene. Thus, it can work entirely in the wild. (2) We propose a memory-efficient solution for differentiable forward rendering and backward propagation. Our framework can directly optimize real-world scene parameters in an iterative and stochastic fashion. (3) Our method can also enable several photo-realistic applications such as novel view synthesis, en-

vironment light editing, etc.

2. PROPOSED METHOD

We illustrate our proposed framework in Fig. (1): It takes a set of RGB images $I = \{I_k\}$ of the scene from arbitrary view-points and camera position as input. Then, our method builds a virtual scene that roughly matches real world camera poses, and iteratively optimize interested scene parameters for 3D geometry, diffuse and specular reflectance, and environment lighting by pushing the photometric consistency between rendering images and real photography. Finally, a set of optimized scene parameters can enable several photo-realistic applications: view synthesis, lighting editing, etc. Mathematically, our system can be described as a function of desired parameters as,

$$I = \Phi(\theta_g, \theta_d, \theta_s, \theta_l), \quad (1)$$

where Φ is the physically-based rendering process, which simulates the light rays traveling in a virtual scene. $\theta_g = \{x_0, \dots, x_N\}$ is the set of 3D positions corresponding to the mesh vertices. $\theta_d = \{\theta_d(x_0), \dots, \theta_d(x_N)\}$ is the set of diffuse per-vertex color reflectance, with $\theta_d(x) \in \mathbb{R}^3$. Similarly, θ_s is the set of specular reflectances. The illumination in the scene is modeled as environmental lighting l_0 , approximated as a set of isotropic point sources $\theta_l = \{l_0, l_1, \dots, l_M\}$, l_n is the intensity for n -th light sources. We use Mitsuba2 [20] as our physically-based rendering engine and renderer. Therefore, it enables an iterative optimization pipeline that back-propagates rendering error to update scene parameters.

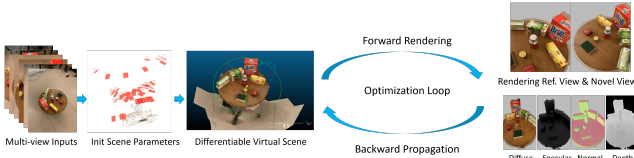


Fig. 1. Inverse parameter optimization pipeline.

Our image formation model for each 2D pixel coordinate u can be formulated as

$$I(u) = L(w_o; x) \Delta t, \quad (2)$$

where $x \in \mathbb{R}^3$ is the 3D coordinate, and $u \in \mathbb{R}^2$ is the 2D image coordinate. $L(w_o; x)$ is the radiance from reflected scene point x with outgoing direction w_o . Δt is the exposure time. According to rendering equation [21], the radiance of a non-emitting object can be written as

$$L_o(w_o; x) = \int_{\Omega} f_r(x, w_i, w_o) L_i(w_i; x) (w_i \cdot n(x)) dw_i, \quad (3)$$

where $L_i(w_i; x)$ and $L_o(w_o; x)$ are the incoming and outgoing radiance functions with direction w_o and w_i for a 3D

physical point x . $n(x)$ is the normal function. Ω is the ray direction space. f_r is physical or estimated reflectance model.

In our virtual scene, an environment light source emits light to the virtual scene and bounces when hitting a 3D object. This environment light is represented as a set of isotropic point sources. Let x' be the 3D position of one of the environment light point sources. The ray tracing can be described by an iterative process. First, light rays originate at an environment light source as

$$L^0(w_i; x) = \theta_l(x'), \quad (4)$$

where the superscript notes the 0-th bounce of light. We assume that environment light is an isotropic light. Thus, the intensity is identical for any incoming direction w_i , i.e., $x' \rightarrow x$. When the light ray hitting the 3D object in the scene, $L_i^t(w_o; x)$ is the t -th bounce of outgoing light ray that directly hits camera aperture, and other reflected light with a different direction than w_o will start a new bounce until reaching a maximal bounce limit.

$$L_o^t(w_o; x) = \int_{\Omega} f_r(x, w_i, w_o) L_i^{t-1}(w_i; x) (w_i \cdot n(x)) dw_i, \quad (5)$$

the overall radiance received by the camera is the sum over all outgoing light, and a maximum of T bounces:

$$L_o(w_o; x) = \sum_{t=0}^T L_o^t(w_o; x), \quad (6)$$

We assume that our scene contains a rough surface with diffuse and specular reflection without transmission, and Cook-Torrance (CT) model [22] with an optional microfacet distribution function, e.g., Beckmann [22], GGX [23], can describe a broad class of general real-world objects in reflection. Our reflectance model f_r can be expressed as follows:

$$f_r(x, w_i, w_o) = \theta_d(x) + \theta_s(x, w_i, w_o), \quad (7)$$

$$\theta_d(x) = \frac{\rho_d(x)}{\pi}, \quad (8)$$

$$\theta_s(x, w_i, w_o) = \rho_s(x) \frac{D(h, \alpha) G(n(x), w_i, w_o) F(h, w_i)}{4(n(x) \cdot w_i)(n(x) \cdot w_o)}, \quad (9)$$

where θ_d and θ_s are diffuse and specular reflectance respectively, ρ_d and ρ_s are diffuse and specular albedos, h is the halfway vector, which is computed by normalizing the sum of the light direction w_i and view direction vectors w_o . Our $D(h, \alpha)$ is the microfacet distribution function. α specifies the roughness of surface micro-geometry along with the tangent and bitangent directions. G is a shadowing-masking function, and F is the Fresnel term similar in [23]. Thus, we reach our rendering function by combining Eqn. (2), Eqn. (3), Eqn. (7) as,

$$I(u) = \Phi(\theta_g, \theta_d, \theta_s, \theta_l)(x) = \Delta t \sum_{t=0}^T L_o^t(w_o; x), \quad (10)$$

$$I(u) = \Delta t \sum_{t=0}^T \int_{\Omega} (\theta_d(x) + \theta_s(x)) L_i^{t-1}(w_i; x) (w_i \cdot n(x)) \, dw_i, \quad (11)$$

$L_i^{t-1}(w_i; x)$ is incoming radiance from every possible direction with a bounce number of $t - 1$, which is also an integral over the bounce number of $t - 2$. For the case of $t = 0$ in Eqn. (4), $L^0(w_i; x)$ is initial environment lighting θ_l .

Our objective function aims at jointly reconstructing the diffuse reflectance θ_d and specular reflectance θ_s , 3D geometry θ_g for mesh and environment light source θ_l .

$$\mathcal{O} = \sum_{k=1}^K \|M_k I_k - \Phi_k(\theta_g, \theta_d, \theta_s, \theta_l)\|_2^2. \quad (12)$$

Rendering results only contain the target object without background, and thus the error of the background pixels will dominate objective value. To alleviate this effect, M_k is a pre-computed binary mask that removes background pixel contribution in the objective calculation, generated by segmentation methods GrabCut [24] and [25] for view consistency. We implement our differentiable optimization pipeline in Mitsuba2 [20] by using forward rendering and backward propagation manner and initial parameters by colmap. Due to the limited GPU memory, we alternate between updating each parameter while keeping the others unchanged. By choosing one scene parameters $\theta \in \{\theta_d, \theta_g, \theta_s, \theta_l\}$, we iteratively update chosen θ in the inner loop.

3. EXPERIMENTS AND COMPARISON

We take photo for the target scene from multiple viewpoints (20-40) with an auto-focus setup, without extra controlled lighting or flash, ordinary ambient light or direct, diffuse light is sufficient. At the initial stage, we set the radiance of the light source to be 0.5. Physically-based rendering is a GPU memory-consuming task, and we adjust several parameters for the sake of memory saving. We set the maximum number of bounce $T = 3$ for ray tracing bounce number, and raw images are downsampled for $8\times$, the number of sampling per pixel $spp = 1$ in iterative optimization stage, and $spp = 16$ for final output with better visual quality. We use Adam as our optimizer, as $\lambda_d = 0.1$, $\lambda_g = 0.5$, $\lambda_s = 0.01$, $\lambda_l = 0.05$ as learning rate. $\alpha = 0.1$ for general surface roughness. Our proposed method runs around 140ms per iteration, 400 iterations to optimize a viewpoint.

3.1. Evaluation and comparison

In this section, we compare our method against other SOTA methods visually and quantitatively. Fig. (2) shows reconstructed scenes and novel view rendering. Our novel view rendering can successfully recover true 3D geometry of the

scene, accurate texture and details of objects, the photo-realistic glossy reflection of the surface. Fig. (3) shows the recovered components of diffuse and specular reflectance, novel views, generated depth, and surface normal.

For visual comparison in Fig. (6), our input images contain significant viewpoint changes and various captured distances, NeRF [16] have leaking light phenomenon in a long range view, due to less novel view direction sampling. We render Colmap [11, 12]’s output textured mesh in renderer, thus, as anticipated, rendering results with decent 3D structures but less accurate surface reflectance can be acquired. PixelNeRF [17] successfully reconstructs 3D geometry with various camera distances using a pretrained network, but still has poor performance in recovering detail textures. NeRF-based methods apply implicit volume to describe diffuse/specular reflection real scene, without taking multiple bounce of light and geometry cues for solving inverse rendering problem. In contrast, our differentiable pipeline directly optimizes the scene parameter to match the real scene image. Therefore, it can accurately achieve photo-realistic high-quality performance in these viewpoint synthesis scenarios.

In Fig. (7), we test our method with other SOTA methods by using public dataset DTU. As anticipated, colmap [11] show inaccurate texture recovery, pixelNeRF [17] will blur the rendering images with inaccurate lighting since it only use several views as inputs. NeRF [16] successfully recover near view scene in DTU cases, however, slightly blur the synthetic view, while our method performs better in details recovery. In Fig. (5), we visualize the effect of our pipeline for optimizing surface and correct geometry error by utilizing multi-view inverse rendering. We also show relighting results by adding several type of light sources (point light, directional light, diffuse light) with different light positions and viewing angles in Fig. (4). The quantitative evaluation with PSNR and SSIM measurements between synthetic novel view and the captured image is shown in Tab. 1.

	Fruit		Table 1	
	PSNR↑	SSIM↑	PSNR↑	SSIM↑
NeRF	14.35	0.28	15.65	0.32
PixelNeRF	26.25	0.91	26.35	0.84
Colmap	17.51	0.70	18.67	0.75
Initial	17.51	0.70	18.67	0.75
Diff Opt.	26.31	0.82	27.21	0.85
Geo Opt.	27.42	0.93	27.45	0.86
Spe Opt.	27.45	0.94	27.95	0.87
Light Opt.	28.78	0.95	28.03	0.87
Ours	29.02	0.96	28.45	0.88

Table 1. PSNR&SSIM evaluations for comparison.



Fig. 2. Full scene reconstruction. Two scenes are shown: Fruit (Row 1) and Table 2 (Row 2). Column 1, 3 is real captured images, column 2, 4 is corresponding virtual view, column 5-8 are rendering synthetic novel views.

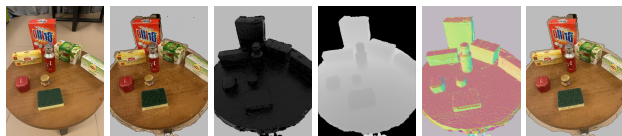


Fig. 3. Reconstruction Components. From left to right: real scene photography, diffuse reflectance θ_d , specular reflectance θ_s , depth map, shading normal, rendering scene.



Fig. 4. Relighting. R1: point light source with fixed position. R2: directional + ambient light. R3: various directional light.

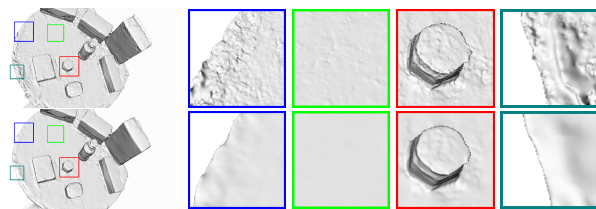


Fig. 5. Surface Refinement. R1: original geometry, R2: optimized geometry. Our method can significantly correct local geometry error in feature matching.

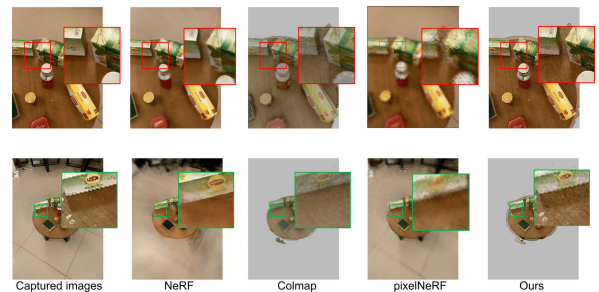


Fig. 6. Viewpoint synthesis for various camera poses and range. From left to right: captured images (Table 1), NeRF results [16], Colmap [12], pixelNeRF [17] and Ours.

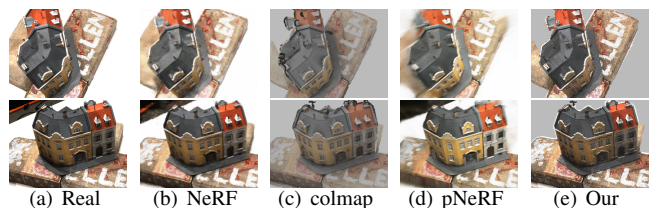


Fig. 7. Visual comparison on DTU[26] dataset.

4. CONCLUSION

We propose a novel differentiable optimization framework that simultaneously reconstructs scene parameters: diffuse and specular reflectance, geometry, environment lighting using the hand-held camera from an uncontrolled environment. Our method can handle a wide range of materials and general ambient lighting, offers an attractive and efficient solution, facilitating in-the-wild scene reconstruction for a wider public, enables various applications: photo-realistic view synthesis, 3D geometry optimization, depth estimation, lighting editing.

5. REFERENCES

- [1] Shichen Liu, Tianye Li, Weikai Chen, and Hao Li, “Soft rasterizer: A differentiable renderer for image-based 3d reasoning,” in *Proc. ICCV*, 2019.
- [2] Xingyuan Sun, Jiajun Wu, Xiuming Zhang, Zhoutong Zhang, Chengkai Zhang, Tianfan Xue, Joshua Tenenbaum, and William Freeman, “Pix3d: Dataset and methods for single-image 3d shape modeling,” in *Proc. CVPR*, 2018.
- [3] Jason Geng, “Structured-light 3d surface imaging: a tutorial,” *Advances in Optics and Photonics*, 2011.
- [4] SC Chan, Heung-Yeung Shum, and King-To Ng, “Image-based rendering and synthesis,” *SPM*, 2007.
- [5] Cha Zhang and Tsuhan Chen, “A survey on image-based rendering—representation, sampling and compression,” *Signal Processing: Image Communication*, 2004.
- [6] Zhong Liu, Zhouchi Lin, Xiguang Wei, and Shing-Chow Chan, “A new model-based method for multi-view human body tracking and its application to view transfer in image-based rendering,” *TMM*, 2017.
- [7] Zhengqin Li, Mohammad Shafiei, Ravi Ramamoorthi, Kalyan Sunkavalli, and Manmohan Chandraker, “Inverse rendering for complex indoor scenes: Shape, spatially-varying lighting and svbrdf from a single image,” in *Proc. CVPR*, 2020.
- [8] Fujun Luan, Shuang Zhao, Kavita Bala, and Zhao Dong, “Unified shape and svbrdf recovery using differentiable monte carlo rendering,” in *Proc. EGSR*, 2021.
- [9] Marc-Andre Gardner, Yannick Hold-Geoffroy, Kalyan Sunkavalli, Christian Gagne, and Jean-Francois Lalonde, “Deep parametric indoor lighting estimation,” in *Proc. ICCV*, 2019.
- [10] V. Gkitsas, N. Zioulis, F. Alvarez, D. Zarpalas, and P. Daras, “Deep lighting environment map estimation from spherical panoramas,” in *Proc. CVPR Workshop*, 2020.
- [11] Johannes Lutz Schönberger and Jan-Michael Frahm, “Structure-from-motion revisited,” in *Proc. CVPR*, 2016.
- [12] Johannes Lutz Schönberger, Enliang Zheng, Marc Pollefeys, and Jan-Michael Frahm, “Pixelwise view selection for unstructured multi-view stereo,” in *Proc. ECCV*, 2016.
- [13] Daniel Maurer, Yong Chul Ju, Michael Breuß, and Andrés Bruhn, “Combining shape from shading and stereo: A joint variational method for estimating depth, illumination and albedo,” *IJCV*, 2018.
- [14] Justus Thies, Michael Zollhöfer, and Matthias Nießner, “Deferred neural rendering: Image synthesis using neural textures,” in *ACM Trans. Graph.*, 2019.
- [15] Vincent Sitzmann, Michael Zollhöfer, and Gordon Wetzstein, “Scene representation networks: Continuous 3d-structure-aware neural scene representations,” in *Proc. NeurIPS*, 2019.
- [16] Ben Mildenhall, Pratul P. Srinivasan, Matthew Tancik, Jonathan T. Barron, Ravi Ramamoorthi, and Ren Ng, “Nerf: Representing scenes as neural radiance fields for view synthesis,” in *Proc. ECCV*, 2020.
- [17] Alex Yu, Vickie Ye, Matthew Tancik, and Angjoo Kanazawa, “pixelNeRF: Neural radiance fields from one or few images,” in *Proc. CVPR*, 2021.
- [18] Lingjie Liu, Jiatao Gu, Kyaw Zaw Lin, Tat-Seng Chua, and Christian Theobalt, “Neural sparse voxel fields,” *Proc. NeurIPS*, 2020.
- [19] Jonathan Barron, Ben Mildenhall, Matthew Tancik, Peter Hedman, Ricardo M. B., and Pratul P. Srinivasan, “Mip-nerf: A multiscale representation for anti-aliasing neural radiance fields,” in *Proc. ICCV*, 2021.
- [20] Merlin Nimier-David, Delio Vicini, Tizian Zeltner, and Wenzel Jakob, “Mitsuba 2: A retargetable forward and inverse renderer,” *ACM Trans. Graph.*, 2019.
- [21] James T. Kajiya, “The rendering equation,” in *Siggraph*, 1986.
- [22] R. L. Cook and K. E. Torrance, “A reflectance model for computer graphics,” *ACM Trans. Graph.*, 1982.
- [23] Bruce Walter, Stephen R. Marschner, Hongsong Li, and Kenneth E. Torrance, “Microfacet models for refraction through rough surfaces,” in *Eurographics Conference on Rendering Techniques*, 2007.
- [24] Carsten Rother, Vladimir Kolmogorov, and Andrew Blake, “Grabcut: interactive foreground extraction using iterated graph cuts,” *ACM Trans. Graph.*, 2004.
- [25] Rui Li and Wolfgang Heidrich, “Hierarchical and view-invariant light field segmentation by maximizing entropy rate on 4d ray graphs,” in *ACM Trans. Graph.*, 2019.
- [26] Rasmus Jensen, Anders Dahl, George Vogiatzis, Engil Tola, and Henrik Aanæs, “Large scale multi-view stereopsis evaluation,” in *Proc. CVPR*, 2014.